

# Angular Dependence of Vertically Propagating Radio-Frequency Signals in South Polar Ice

DaveZ Besson<sup>1,2</sup>, Ilya Kravchenko<sup>3</sup>, Krishna Nivedita<sup>4</sup>

<sup>1</sup>*Dept. of Physics and Astronomy, Univ. of Kansas, Lawrence, KS, 66044, USA*

<sup>2</sup>*National Research Nuclear University, Moscow Engineering Physics Institute, Moscow, 115409, Russia*

<sup>3</sup>*Dept. of Physics and Astronomy, Univ. of Nebraska-Lincoln, NE, 68588, USA*

<sup>4</sup>*Indian Institute of Science Education and Research, Thiruvananthapuram, Vithura, Kerala 695551, India*

*Correspondence: DaveZ Besson <zedlam@ku.edu>*

**ABSTRACT.** To better understand the effect of ice properties on the capabilities of radio experiments designed to measure ultra-high energy neutrinos (UHEN), we recently considered the timing and amplitude characteristics of radio-frequency (RF) signals propagating along multi-kilometer, primarily horizontal trajectories through cold Polar ice at the South Pole. That analysis indicated satisfactory agreement with a model of ice birefringence based on  $\hat{c}$ -axis data culled from the South Pole Ice Core Experiment (SPICE). Here we explore the geometrically complementary case of signals propagating along primarily vertical trajectories, using published data from the Askaryan Radio Array (ARA) experiment, supplemented by a re-analysis of older RICE experimental data. The timing characteristics of those data are in general agreement with the same birefringence model. Re-analysis of older RICE data also confirm the correlation of signal amplitudes reflected from internal-layers with the direction of ice flow, similar to previous observations made along a traverse from Dome Fuji to the Antarctic coast. These results have two important implications for radio-based UHEN experiments: i) owing to birefringence, the timing characteristics of signals propagating from neutrino-ice interactions, either vertically or horizontally, to a distant receiver may be used to infer the distance-to-vertex, which is necessary to estimate the energy of the progenitor neutrino, ii) the measured reflectivity of internal layers may result in previously-unanticipated backgrounds to UHEN searches, requiring significantly more modeling and simulations to estimate.

## INTRODUCTION

The field of radio-frequency neutrino detection via the Askaryan Effect(Askaryan, 1962, 1965) has undergone steady, and significant growth since its experimental inception approximately one-quarter century ago. The early 1990's marked the first detailed simulation of the coherent microwave signal expected for in-ice neutrino interactions(Zas and others, 1992), as well as a full-scale experimental simulation(Frichter, George M. and Ralston, John P. and McKay, Douglas W., 1996). Deployment of hardware(Kravchenko and others, 2003; Kravchenko and others, 2006) and test beam experiments(Saltzberg and others, 2001; Gorham and others, 2007) verifying the expected signal followed soon thereafter. The polar ice sheets, comprising a large, stable, and largely homogeneous radio-transparent(Barwick, S., Besson, D., Gorham, P. and Saltzberg, D., 2005) neutrino target comprise an attractive target medium. It has long been realized that the experimental sensitivity of such experiments are ultimately determined by the dielectric properties, particularly refraction, attenuation, and polarization-dependent asymmetries ('birefringence') of the polar ice itself.

Within the last several years, both modeling and some experimental work have indicated unexpected signal propagation modes(Barwick and others, 2018; Deaconu and others, 2018; Prohira and others, 2021), which may impact the scientific mission of planned neutrino observatories. In that case, short-duration (nanosecond-scale) radio-frequency signals propagating over the  $\sim$ km-scale baselines typical of neutrinos may exhibit measurable variations in amplitude over modest differences in reception geometry, otherwise unexpected for a uniform, isotropic target. A rough estimate of the scale of ice density perturbations required to yield observable effects can be obtained from simple arguments. In a ray optics picture, two one-meter wavelength ( $f=300$  MHz) signals traveling in a medium with density (and therefore refractive index) fluctuations of order 1.5 parts per mille shift by  $\delta\phi = \pi/2$  for each 0.25 km of pathlength. In the conventional Huygens wave optics picture, one important implication of such density fluctuations is that the detailed cancellation of wavelets, leading to 'shadow' zones for the case of media with smoothly varying refractive index profiles, is disrupted, resulting in some signal observed from otherwise classically-forbidden source regions (as measured in data)(Barwick and others, 2018). This picture is further complicated by birefringent effects, such that the signal velocity varies with signal polarization.

## BIREFRINGENCE

Absent external stresses, isolated ice crystals have roughly six-fold planar rotational symmetry (Bragg, 1921). Within the ice sheet, ice crystals are subject to strain along both vertical (due to the gravitational overburden) and also horizontal (due to ice flow) directions (Rigsby, 1960; Alley and others, 1995). In the ‘standard’ picture, the  $\hat{c}$ -axis distribution is expected to be approximately isotropic, with no preferred spatial direction, for shallow ice with modest overburdens. At intermediate depths, orientations for which the plane of the ice crystal is perpendicular to the ice flow direction are disfavored; the distribution of vectors normal to the ice crystal plane ( $\hat{c}$ -axes) is correspondingly described as a ‘girdle’, with vertically-stacked ice crystals slightly elongated along the ice flow and the  $\hat{c}$ -axes correspondingly distributed in a plane transverse to the flow direction. At depths closest to the bedrock, the gravitational overburden forces the  $\hat{c}$ -axis to increasingly align with  $\hat{z}$ - to form a uniaxial distribution.

Of particular interest here is the relationship between the measured  $\hat{c}$ -axis distribution and the corresponding expectations for birefringent effects. In our comparison of birefringence data to expectation, we follow the biaxial model developed by Jordan *et al.* (Jordan and others, 2020), based on the South Pole Ice Core Experiment (SPICE) thin slice ice fabric measurements (Voigt, 2017), and data on the light velocity through a crystal, as a function of light polarization axis derived from Fujita *et al.* (Fujita and others, 2003; Matsuoka and others, 1997). Following (Fujita and others, 2003), we designate an orthogonal coordinate system onto which the signal polarization is projected, with basis vectors defined as: the “1-” polarization direction parallel to the ice-flow direction in the horizontal plane, the “3-” direction parallel to  $z$ -, and the “2-” direction perpendicular to the ice-flow direction in the horizontal plane and orthogonal to both “1-” and “3-”. Ice fabric measurements from the SPICE core quantify the degree of alignment of the  $\hat{c}$ -axis with these three directions. For uniaxial laboratory ice, the asymmetry in the refractive index between the 3- direction and the orthogonal 1- or 2- directions is measured to be  $\sim 0.018$  (Matsuoka and others, 1997). For the case of signal propagation in the  $z$ -direction (e.g. as for radar echoes from the Antarctic surface, through the ice, and reflected from the bedrock), the polarization axis lies in the horizontal (1-2) plane. As the signal propagates through the ice, an instantaneous, local coordinate frame is defined by the  $s$ - and  $p$ - polarization vectors, with  $p$ - aligned with the local  $\hat{\theta}$  direction and  $s$ - aligned with the local  $\hat{\phi}$  direction. In this model, for pure horizontal  $k$ -vectors, SPICE  $\hat{c}$ -axis measurements imply that signal polarizations perpendicular to the ice flow direction, and aligned with the 2- axis will temporally lag behind signal polarizations parallel to the ice flow direction.

### Askaryan Radio Array (ARA) SPICE core transmitter calibration data

In 2018-19, a ‘fat’ dipole transmitter was lowered into the ice hole drilled for the South Pole Ice Core Experiment (SPICE); the five Askaryan Radio Array (ARA) receiver stations, ranging from 2–5 km distant and with receivers at 50–200 m depths, recorded time and amplitude signal waveforms (Allison and others, 2020). As reported previously, the measured time asymmetry for propagation along predominantly horizontal trajectories, between polarizations primarily along  $z$ - vs. polarizations in the horizontal plane, is qualitatively consistent with the Jordan *et al.* model (Jordan and others, 2020). For propagation directions parallel to the ice flow direction, the horizontally propagating  $\vec{E}$ -field vector is almost entirely along the 2- direction and the polarization lies in the (2-3) plane; since  $n_2 \approx n_3$ , no time delay is expected between signal arrival times for vertical vs. horizontal polarizations. For propagation directions perpendicular to the ice flow direction, the horizontally propagating  $\vec{E}$ -field vector is almost entirely along the 1- direction, resulting in the VPol signal lagging the HPol signal by some tens of nanoseconds for these baselines, since  $n_1 < n_3$ .

Two effects slightly complicate interpretation of those data: First, as the transmitter antenna is lowered into the SPICE core icehole, the  $p$ -polarization increasingly deviates from true vertical and acquires an increasing horizontal polarization projection component (in addition to the known  $\sim 10$  dB cross-polarization power of the dipole transmitter antenna). Second, we experimentally often observe unexpectedly large power for horizontal polarizations, the origin of which is currently not entirely understood, but may be the result of coupling between the  $s$ - and  $p$ -modes. For the ARA01 station receiver array, for example, corresponding to the steepest incidence angles (approaching 30 degrees with respect to vertical), the measured HPol power has been observed to often exceed the VPol power (Allison and others, 2020); correcting for the more-limited bandwidth of the HPol antennas only exacerbates this excess.

Some of the unexpectedly large HPol power may be a direct consequence of birefringence, as highlighted recently in a more rigorous treatment than Jordan *et al.* (Connolly, 2021). For an isotropic, uniform medium, the local electromagnetic wavespeed is dependent only on the local refractive index profile, independent of both  $\hat{k}$  and polarization  $\hat{P}$ . In a biaxial medium, wavespeed depends on the directional excitation of the ice crystal transporting the signal. For polarizations aligned with  $\hat{1}$ -,  $\hat{2}$ - or  $\hat{3}$ -, the net energy flux vector (Poynting vector  $\hat{S}$ ) measured by an observer is parallel to  $\hat{k}$ . For off-axis signals with polarizations making angles  $\chi_1$ ,  $\chi_2$  and  $\chi_3$  relative to the underlying basis vectors, the non-uniform molecular vibration of the medium ‘projects’ an arbitrary polarization onto the underlying birefringence basis; the transversality condition ( $\vec{E} \times \vec{H} = \hat{k}$ ) which follows from Maxwell’s equations therefore implies that the allowed modes, in general, will have some angular deviation  $\psi$  between  $\hat{k}$  (given by  $\vec{D} \times \vec{B}/\vec{H}$ ) and  $\hat{S}$  (given by  $\vec{E} \times \vec{B}/\vec{H}$ ). Geometrically, whereas in an isotropic medium, energy flows spherically outwards from a given source, in a birefringent medium, the direction of net energy flow expands along embedded ellipsoids, with an angular deviation from spherical flow proportional to the refractive index asymmetry. In the presence of possible interference (and exacerbated by the cross-polarization response of a given antenna), the amplitude of a transmitted continuous wave signal at a receiver will therefore depend on the angles  $\chi_1$ ,  $\chi_2$ ,  $\chi_3$  and the propagation distance. For short-

duration signals, such that the duration  $t_{\text{signal}}$  is much smaller than the combined effects of the intrinsic transmitter, receiver and system electronics response time and group delays  $t_{\text{response}}$ , signal may similarly interfere at the receiver, or in the data acquisition (DAQ) hardware. As the transmitter descends and the signal polarization increasingly inclines relative to vertical, mixing between the p- and s- states permits a greater p-polarization fraction at the transmitter to be measured as s-polarization.

In addition to the SPICE core transmitter, the so-called ‘deep transmitters’ co-deployed with IceCube photomultiplier modules on IceCube strings 1 and 22 in 2011 with the first Askaryan Radio Array (ARA) deployment also provide a ‘standard’ calibration source, as reported elsewhere (Allison and others, 2019; et al., 2012). Two shallower transmitters (IC1S and IC2S) were deployed at a depth of 1400 meters; one transmitter was deployed at a depth of 2400 meters in IceCube hole 1 (IC1D). Ray trajectories to the so-called ‘testbed’ receiver station from IC1D are inclined at nearly 45 degrees relative to the vertical; projected onto the horizontal plane, a ray path from the deep pulsers to the testbed makes an azimuthal angle of approximately 30 degrees with respect to the local horizontal ice flow direction. Unlike the ARA stations deployed subsequent to the testbed deployment, for which antennas were configured into eight HPol/VPol pairs separated by  $\sim 2$  m, the placement of the testbed antennas was less standardized. Into each of four testbed ice boreholes, one HPol and one VPol antenna were deployed, with vertical separations between H and V varying from  $-6 \rightarrow +6$  meters. Numerically, however, we can take advantage of the fact that the summed depth of the four antennas of each polarization are approximately equal (to within 0.5 m), so propagation time differences between HPol/VPol pairs should (modulo refractive index biases) largely cancel; i.e., in the absence of birefringence  $\Sigma_i(t(\text{arrival}_i^{\text{Hpol}}) \approx \Sigma_i(t(\text{arrival}_i^{\text{Vpol}})$ . As reported elsewhere, calculating these sums for the three deep pulsers, we find a per-channel HPol-VPol arrival time separation of  $-7 \rightarrow -9$  ns for all three of the pulsers (Allison and others, 2020). Those values can be reconciled with the Jordan *et al.* model if the  $\hat{c}$ -axis distribution underwent a sharp transition to a uniaxial single-pole below the maximum depth for which SPICE core data were collected (1740 meters).

## DATA TAKEN WITH THE RICE EXPERIMENT

In bistatic radar data taken in 2007 by the RICE experiment, two horn antennas were placed on the South Polar ice surface, with the horn faces directed downwards into the snow (Besson and others, 2009, 2011). As the two horn antennas were co-rotated and ns-duration signals fed into the transmitter horn antenna, echoes were recorded in the receiver horn antenna, resulting from both discrete internal layer as well as continuous volumetric signal scattering. Although not systematically quantified, those data suggested an unexpectedly large variation in signal return strength, as a function of azimuthal angle  $\phi$  relative to the local ice flow direction (approximately 40 degrees west of grid North). The goal of that original analysis was to measure birefringence, as a function of depth, to similarly infer the depth dependence of ice properties. A nearly identical study at Taylor Dome, for example, revealed a measurable,  $\sim 10$ -nanosecond time shift, relative to a total travel time-to-bedrock of  $\sim 11700$  ns, between the fast/slow azimuthal orientations, observed to be perpendicular to each other (Besson and others, 2008). The earlier RICE data, however, indicated simultaneity of echo returns, for all azimuthal orientations, up to 13 microsecond return times, although the analysis at that time still allowed 5–10 ns systematic errors.

Herein, we have conducted a reanalysis of the earlier RICE data using improved signal processing software. For the 2007 RICE data sample, we identify internal layer echoes by their observed (uncorrected for intrinsic cable delays, measured to be  $\sim 190$  ns) return times, corresponding to a bright echo at  $6 \mu\text{s}$  return time, a triplet of echoes between 9.7 and 10 microseconds, a second triplet of echoes between 13.7 and 14 microseconds, and weaker echoes at 17.6 and 19.3 microseconds, respectively.

### Signal wave speed dependence on polarization angle

The greatest fractional temporal resolution obtains from the deepest recorded echo. Figure 1 shows the (normalized) Hilbert transform of the recorded voltage traces, for azimuthal polarizations either parallel or perpendicular to ice flow, with fits to a Gaussian signal plus a first-order polynomial function overlaid. Our revised analysis indicates a temporal shift for polarizations parallel to the ice flow direction relative to polarizations perpendicular to the ice flow direction. Combined with similar measurements for the earlier echoes, as well as bedrock echoes and measurements made at Taylor Dome, Figure 2 overlays our propagation time data points with model predictions from Jordan *et al.* Similar to observations made for horizontally propagating signal, the Jordan *et al.* model qualitatively reproduces the features observed in our data (Jordan and others, 2020). The discrepancy observed for the case of the ARA testbed, we conjecture, is due to the failure of the model for largely-inclined geometries, perhaps due to modal coupling.

### Amplitude dependence on polarization angle

Figure 3 illustrates the correlation of echo strength with azimuthal signal polarization angle; we use a local coordinate system for which the ice flow direction corresponds to  $\phi \approx 60^\circ$ . Previous measurements of signal returns along a traverse from Dome Fuji to the Antarctic coast also revealed a strong dependence of reflected signal amplitude on the signal polarization angle, referenced to the local ice flow direction; the echo return power for polarizations aligned with the local ice flow direction were observed to be  $\sim 10$  dB smaller than for polarizations perpendicular to the local ice flow direction (Matsuoka and others, 2003). Our observations are consistent with that result, as well as a preliminary version of this analysis (Besson and Kravchenko, 2013).

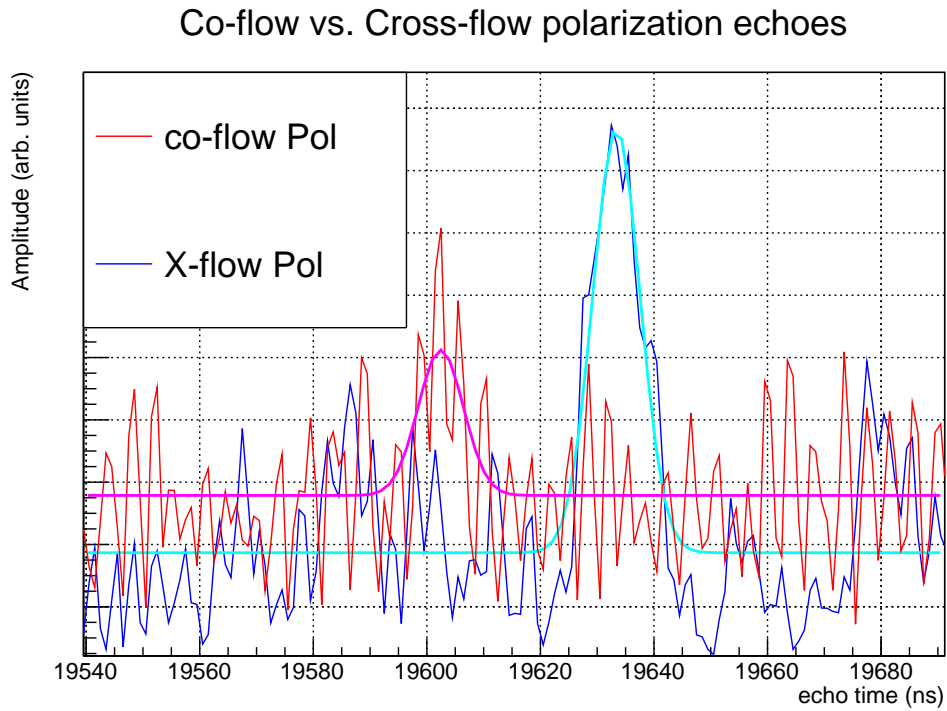


**Fig. 1.** Hilbert Transform of radar echo voltage traces, measured around  $19.6 \mu\text{s}$  return time. Overlaid are Gaussian fits to most significant excursions for polarizations aligned either along- or transverse to flow direction, as indicated in Figure.

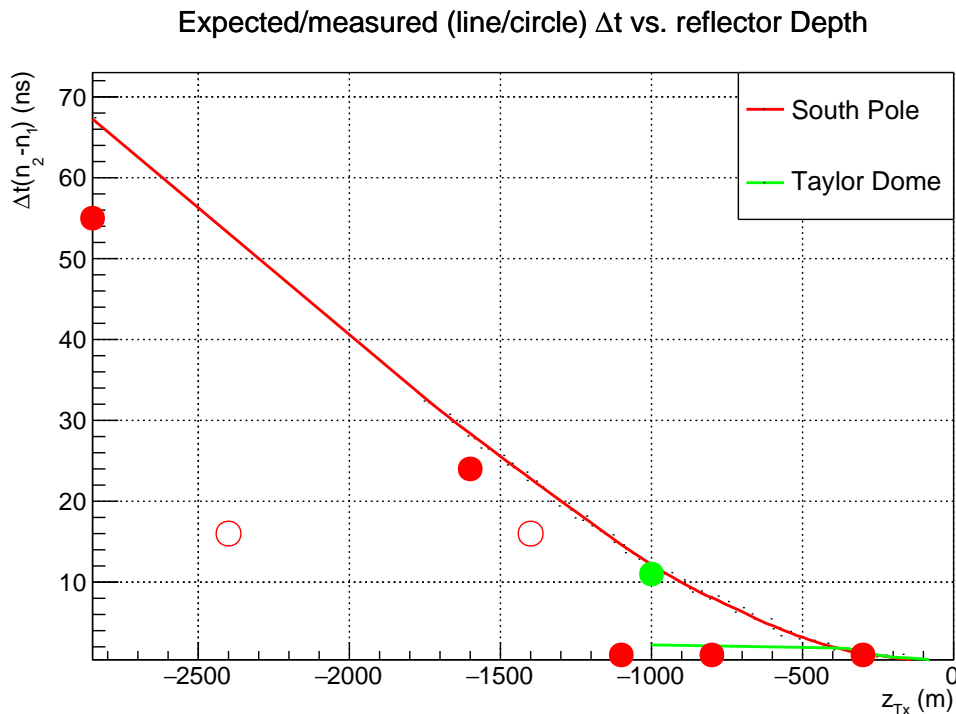


**Fig. 2.** Predicted (line, based on Jordan *et al.* model) vs. measured (circles) birefringent time difference for both South Pole (red) and also Taylor Dome (green). Prediction is based on SPICE ice fabric measurements to a depth of 1700 meters; shown curve for  $z < -1700$  m assumes a linear extrapolation to the bedrock. A more realistic extrapolation would take into account the expected transition to a single-pole uniaxial c-axis orientation in the lower third of the ice sheet. Filled red circles are derived from RICE data; open red circles are published results from Askaryan Radio Array (ARA). Estimated systematic errors on raw time difference data points shown as circles are approximately 1-2 nanoseconds.

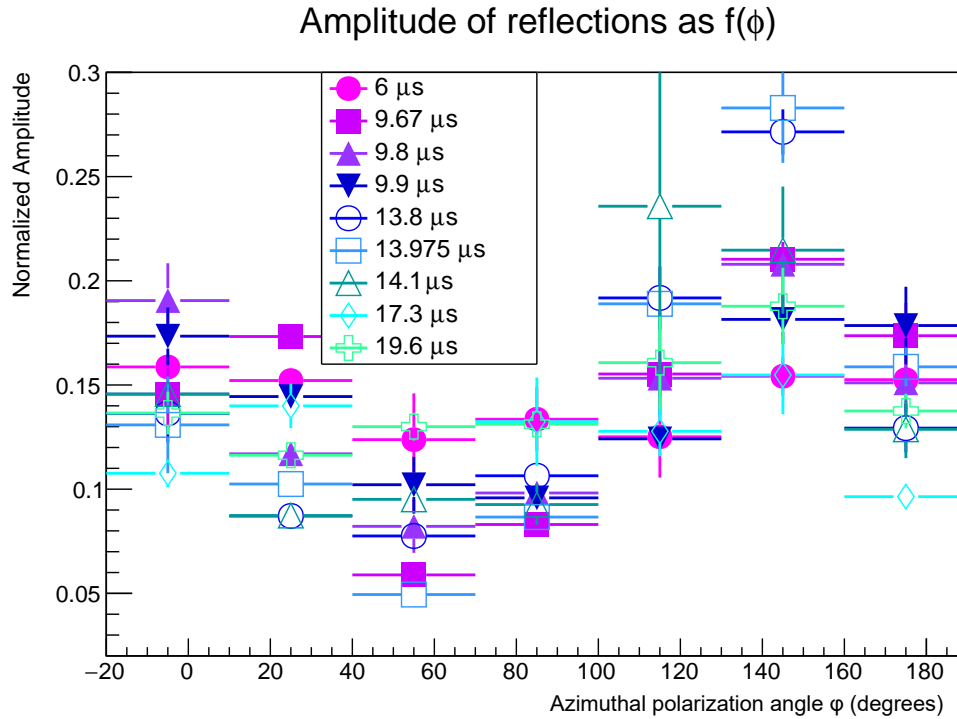


**Fig. 3.** Peak measured amplitude dependence of internal layer echoes on azimuthal signal polarization angle  $\phi$ , as measured in horizontal plane.

Figure 4 shows the bedrock return for signal polarizations at 45 degrees relative to the local ice flow direction (Besson and others, 2011). Both the fast and slow bedrock echoes have comparable amplitudes, indicating that the amplitude dependence observed for internal layer scattering is a direct consequence of the scatterer itself, with a mechanism distinct from reflections at the ice/bedrock interface.

### Estimate of internal layer reflection strength

Although not an original goal of the RICE echo layer measurements, we have attempted to estimate the absolute reflectivity of each layer. This is particularly important for current UHEN-detection experiments with estimated detection rates of order 1 per 10 years, since down-coming radio signals from either natural or anthropogenic origin may reflect upwards from an underlying embedded in-ice layer, yielding signatures otherwise indistinguishable from those of the sought-after neutrinos. The Friis Equation (Shaw, 2013) prescribes the wavelength-dependent received power  $P_{Rx}(\lambda)$  given the power output from a transmitter  $P_{Tx}(\lambda)$  in the frequency band overlapping with the receiver frequency response, for propagation through a distance  $d$  in a medium with frequency-dependent attenuation length  $L_\alpha$ :

$$P_{Rx}(\lambda) = P_{Tx}(\lambda) \mathcal{G}_{Tx} \mathcal{G}_{Rx} f_{focus} F_{Fresnel} \left( \frac{\lambda}{4\pi d^2} \right) \exp(-d/L_\alpha);$$

here,  $\lambda$  is the wavelength being broadcast (here, taken to be 1 meter, although the broadcast pulse is, in fact, broadband),  $\mathcal{G}_{Tx}$  and  $\mathcal{G}_{Rx}$  refer to the gain of the transmitter and receiver, respectively, and  $f_{focus}$  represents a geometric flux focusing factor. For the case of reflection, we must introduce the so-called radar cross-section ('RCS')  $\sigma_{RCS}$ . In that case, for bistatic measurement of a reflecting layer a distance  $d$  from transmitter, we obtain:

$$P_{Rx}(\lambda) = P_{Tx}(\lambda) \mathcal{G}_{Tx} \mathcal{G}_{Rx} f_{focus} F_{Fresnel} \left( \frac{\lambda}{4\pi d^2} \right) \exp(-2d/L_\alpha) \times \left( \frac{\sigma_{RCS}}{4\pi d} \right)^2;$$

with  $F_{Fresnel}$  an angular-dependent Fresnel coefficient; this equation reduces to the Friis equation if the scattering cross-section equals  $4\pi d^2$  (reflection of all the output power) and  $F_{Fresnel} \equiv 1$ . In our case, we take the scattering cross-section to be equal to one Fresnel zone at the distance  $d$ :  $\sigma_{RCS} = \pi \lambda d^2 / 2d$ , which affords an estimate of the absolute scattering power of each layer.

Results are summarized in Figure 5. Typical peak (corresponding to  $\phi \sim 150$  degrees) reflection coefficients are of order -50 - -60 dB, although systematic errors are estimated to be  $\pm 12$  dB per point. The dominant systematic error is the uncertainty in the bandpass overlap between the transmitted signal and the received signals. Our results are qualitatively consistent with previously reported observations of layer echoes in polar icesheets from both Antarctica and Greenland at a variety of sites and layer depths, as summarized in Table 1.

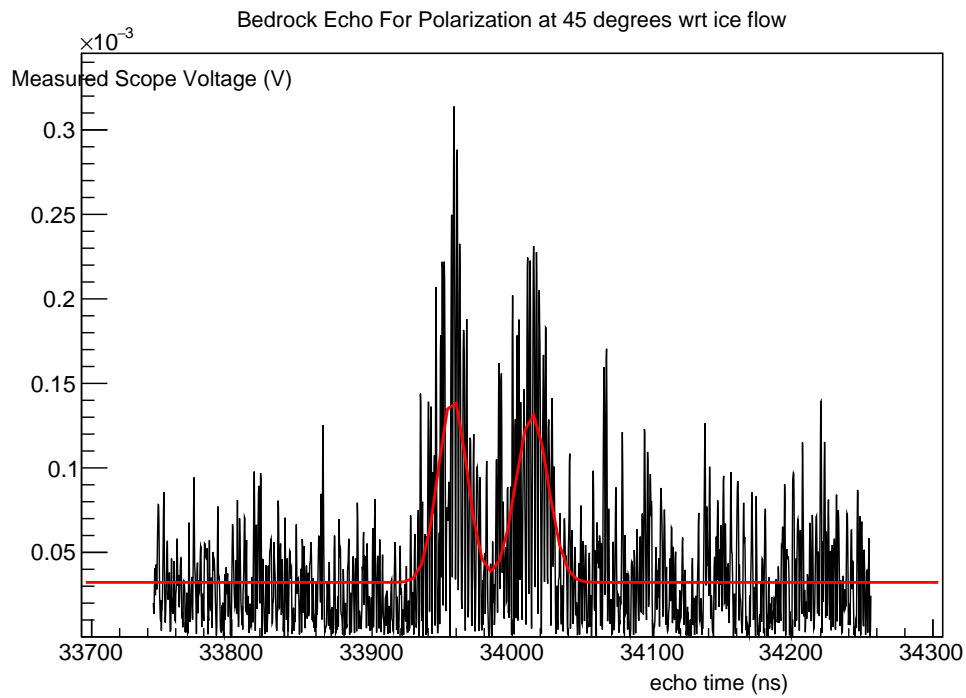


**Fig. 4.** Measured South Pole bedrock echo signal power, as function of time, for polarization at 45 degrees w.r.t. ice flow direction, showing both the fast (early) and slow (later) echo returns. Overlaid is fit to double Gaussian signal plus flat background.

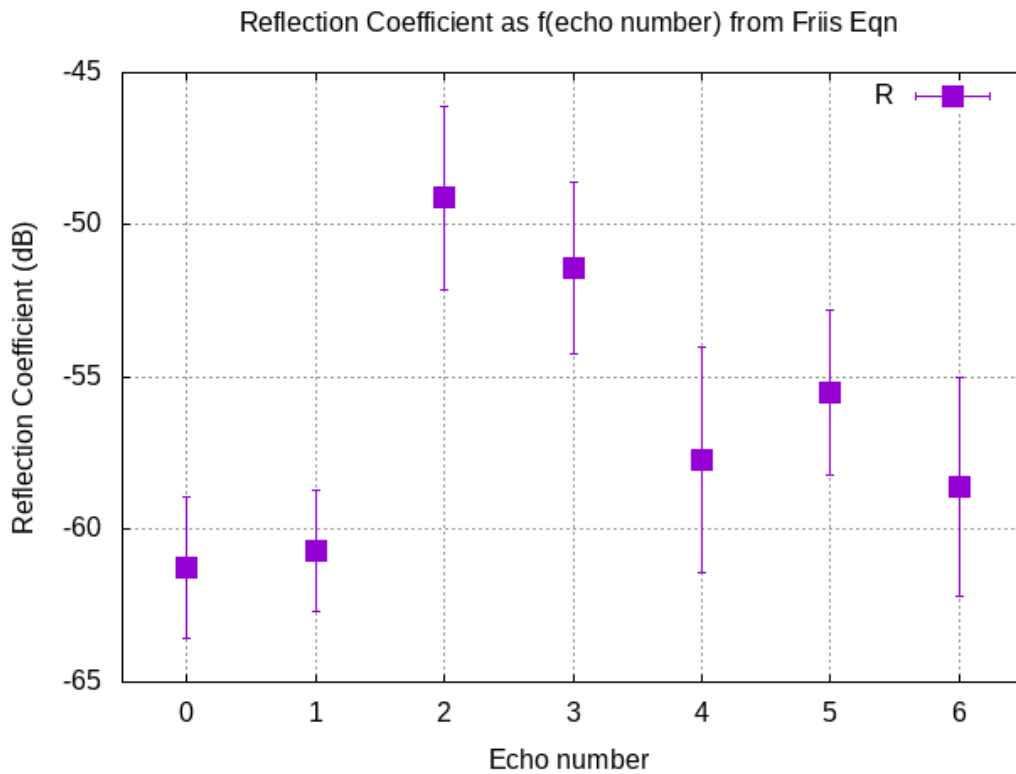


**Fig. 5.** Peak layer power reflection coefficient, calculated from radar equation (Shaw, 2013). Correlation between echo number and return time is: 0: 6  $\mu$ s; 1-3: triplet between 9.67 and 9.9  $\mu$ s; 4-6: triplet between 13.8 and 14.1  $\mu$ s. Displayed errors are statistical only; systematic errors are estimated at  $\pm 12$  dB per point.

site	depth(m)	$f_0$ (MHz)	pulse duration (ns)	$P_0$ (W)	$\mathcal{R}$ (dB)
Tuto-Camp Century(Bailey and others, 1964) (G)	420-610	35 MHz	240 ns	50 W	-43 – -70
near Camp Century(Robin and others, 1969) (G)	410-455	35 MHz	240 ns	50 W	-72 – -80
Crete(Preben, 1975) (G)	2300-2500	60 MHz	250ns	10kW	-70 – -75
Byrd station(Robin and others, 1970)	1250	35MHz	240ns	500W	-69
Sovetskaya(Robin and others, 1970)	<2200	35MHz	240ns	500W	-76
South Pole(Harrison, 1973)	2000-3000	60MHz	1000ns	800W	-75

**Table 1.** Summary of internal layer reflection coefficients measurements at variety of Greenland (indicated by “(G)”) and Antarctic sites. Center frequency  $f_0$ , pulse duration and power output  $P_0$  of radar system are as shown, as well as measured reflection coefficient  $\mathcal{R}$ .

## SUMMARY AND CONCLUSIONS

Based on an improved analysis of vertical radar echo data taken at the South Pole in 2007 and 2009, and previously reported results, we summarize our conclusions as follows:

1. Complementing previous measurements at largely horizontal launch angles, we have measured birefringent asymmetries for signal propagating along  $\hat{z}$  over multi-kilometer distances, reflecting from both internal layers and the bedrock, finding reasonable agreement for time delays with a model based on ice-fabric measurements. Taken together, these measurements indicate that the distance to vertex between a receiver and source interaction point with an estimated precision of order 15%.
2. We measure the angular dependence of internal layer echo returns, as a function of the azimuthal polarization, and find an order-of-magnitude difference between the signal power returned for the case where the polarization is parallel to the ice flow direction, relative to the case where the polarization is perpendicular to the ice flow direction. This result is consistent with previous measurements made along a traverse from Dome Fuji to the Antarctic coast.
3. Using the Friis equation, we have made an estimate of the absolute reflectivity of several internal layers, obtaining values typically ranging from  $-50 \rightarrow -65$  dB, but with attendant systematic errors of  $\pm 12$  dB.

In order to quantify the impact of these measurements on current and planned UHEN experiments, detailed simulations of a variety of physics processes are required. Such simulations are currently underway. Refinement of these measurements would benefit from improved signal transmission, and, perhaps most importantly, higher bandwidth and sampling-rate data acquisition hardware. It is hoped that such a campaign may be conducted at the South Pole in one of the upcoming field seasons.

## ACKNOWLEDGMENTS

IK and DZB thank the National Science Foundation for their generous support of the IceCube EPSCoR Initiative (Award ID 2019597).

## REFERENCES

- Alley RB, Gow A and Meese D (1995) Mapping c-axis fabrics to study physical processes in ice. *Journal of Glaciology*, **41**(137), 197–203
- Allison P and 10 others (2019) Measurement of the real dielectric permittivity  $\epsilon_r$  of glacial ice. *Astroparticle Physics*, **108**, 63–73
- Allison P and 10 others (2020) Long-baseline horizontal radio-frequency transmission through polar ice. *Journal of Cosmology and Astroparticle Physics*, **2020**(12), 009
- Askaryan G (1962) Excess negative charge of an electron-photon shower and its coherent radio emission. *Soviet Physics JETP*, **14**, 441–443
- Askaryan GA (1965) Coherent Radio Emission from Cosmic Showers in Air and in Dense Media. *Soviet Phys. JETP*, **21**, 658
- Bailey J, Evans S and Robin GdQ (1964) Radio echo sounding of polar ice sheets. *Nature*, **204**(4957), 420–421
- Barwick S and 10 others (2018) Observation of classically forbidden electromagnetic wave propagation and implications for neutrino detection. *Journal of Cosmology and Astroparticle Physics*, **2018**(07), 055
- Barwick, S, Besson, D, Gorham, P and Saltzberg, D (2005) South Polar in situ radio-frequency ice attenuation. *Journal of Glaciology*, **51**(173), 231–238
- Besson D and Kravchenko I (2013) Radio-frequency probes of Antarctic ice at South Pole. *CRYOSPHERE*, **7**(3), 855–866, ISSN 1994-0416 (doi: {10.5194/tc-7-855-2013})
- Besson D and 10 others (2008) In situ radioglaciological measurements near Taylor dome, Antarctica and implications for ultra-high energy (uhe) neutrino astronomy. *Astroparticle Physics*, **29**(2), 130–157
- Besson D, Keast R and Velasco R (2009) In situ and laboratory studies of radiofrequency propagation through ice and implications for siting a large-scale Antarctic neutrino detector. *Astropart. Phys.*, **31**, 348–358 (doi: 10.1016/j.astropartphys.2009.03.009)

- Besson D, Kravchenko I, Ramos A and Remmers J (2011) Radio Frequency Birefringence in South Polar Ice and Implications for Neutrino Reconstruction. *Astropart. Phys.*, **34**, 755–768 (doi: 10.1016/j.astropartphys.2011.01.008)
- Bragg W (1921) The crystal structure of ice. *Proceedings of the Physical Society of London (1874-1925)*, **34**(1), 98
- Connolly A (2021) Impact of biaxial birefringence on signal polarization in radio detection of neutrinos in polar ice. *arXiv preprint arXiv:2110.09015*
- Deaconu C and 8 others (2018) Measurements and modeling of near-surface radio propagation in glacial ice and implications for neutrino experiments. *arXiv preprint arXiv:1805.12576*
- et al PA (2012) Design and initial performance of the Askaryan Radio Array prototype EeV neutrino detector at the South Pole. *Astroparticle Physics*, **35**(7), 457–477
- Frichter, George M and Ralston, John P and McKay, Douglas W (1996) On radio detection of ultrahigh-energy neutrinos in Antarctic ice. *Phys. Rev.*, **D53**, 1684–1698 (doi: 10.1103/PhysRevD.53.1684)
- Fujita S, Matsuoka K, Maeno H and Furukawa T (2003) Scattering of vhf radio waves from within an ice sheet containing the vertical-girdle-type ice fabric and anisotropic reflection boundaries. *Annals of Glaciology*, **37**, 305–316
- Gorham PW, Barwick SW, Beatty JJ and et al (2007) Observations of the Askaryan Effect in Ice. *Phys. Rev. Lett.*, **99**, 171101 (doi: 10.1103/PhysRevLett.99.171101)
- Harrison C (1973) Radio echo sounding of horizontal layers in ice. *Journal of glaciology*, **12**(66), 383–397
- Jordan TM and 6 others (2020) Modeling ice birefringence and oblique radio wave propagation for neutrino detection at the south pole. *Annals of Glaciology*, **61**(81), 84–91
- Kravchenko I and 17 others (2003) Performance and simulation of the RICE detector. *Astropart. Phys.*, **19**, 15–36
- Kravchenko I and 1 others (2006) Rice limits on the diffuse ultrahigh energy neutrino flux. *Phys. Rev.*, **D73**, 082002 (doi: 10.1103/PhysRevD.73.082002)
- Matsuoka K and 6 others (2003) Crystal orientation fabrics within the antarctic ice sheet revealed by a multipolarization plane and dual-frequency radar survey. *Journal of Geophysical Research: Solid Earth*, **108**(B10)
- Matsuoka T, Fujita S, Morishima S and Mae S (1997) Precise measurement of dielectric anisotropy in ice ih at 39 ghz. *Journal of Applied Physics*, **81**(5), 2344–2348
- Preben G (1975) Layer echoes in polar ice sheets. *Journal of Glaciology*, **15**(73), 95–101
- Prohira S and 9 others (2021) Modeling in-ice radio propagation with parabolic equation methods. *Physical Review D*, **103**(10), 103007
- Rigsby GP (1960) Crystal orientation in glacier and in experimentally deformed ice. *Journal of Glaciology*, **3**(27), 589–606
- Robin GdQ, Evans S and Bailey JT (1969) Interpretation of radio echo sounding in polar ice sheets. *Philosophical Transactions of the Royal Society of London. Series A, Mathematical and Physical Sciences*, **265**(1166), 437–505
- Robin GdQ, Swithinbank C, Smith B and 3 others (1970) Radio echo exploration of the antarctic ice sheet. *International Association of Scientific Hydrology Publication*, **86**, 97–115
- Saltzberg D, Gorham P, Walz D and et al (2001) Observation of the Askaryan Effect: Coherent Microwave Cherenkov Emission from Charge Asymmetry in High-Energy Particle Cascades. *Phys. Rev. Lett.*, **86**, 2802–2805
- Shaw JA (2013) Radiometry and the friis transmission equation. *American journal of physics*, **81**(1), 33–37
- Voigt DE (2017) c-Axis Fabric of the South Pole Ice Core, SPC14. U.S. Antarctic Program (USAP) Data Center. Dataset. (doi: doi:10.15784/601057)
- Zas E, Halzen F and Stanev T (1992) Electromagnetic pulses from high-energy showers: Implications for neutrino detection. *Phys. Rev. D*, **45**, 362–376